Methods in Molecular Biology

Probing single virus binding sites on living mammalian cells using AFM

Martin Delguste*, Melanie Koehler*, David Alsteens

Université catholique de Louvain, Institute of Life Sciences, Louvain-la-Neuve, Belgium

* M.D. and M.K. equally contributed to this work.

Correspondence to: (D.A.) david.alsteens@uclouvain.be

Abstract

The last years, atomic force microscopy (AFM)-based approaches have evolved into a powerful multiparametric tool that allows biological samples ranging from single receptors to membranes and tissues to be probed. Force-distance curve-based AFM (FD-based AFM) nowadays enables to image living cells at high-resolution and simultaneously localize and characterize specific ligand-receptor binding events. In this chapter, we present how FD-based AFM permits to investigate virus binding to living mammalian cells and quantify the kinetic and thermodynamic parameters that describe the free-energy landscape of the single virus binding. Using a model virus, we probed the specific interaction with cells expressing its cognate receptor and measured the affinity of the interaction. Furthermore, we observed that the virus rapidly established specific multivalent interactions and found that each bond formed in sequence strengthens the attachment of the virus to the cell.

Keywords

nanoscopy, microscopy, scanning probe microscopy, atomic force microscopy, AFM, single-molecule force spectroscopy, confocal microscopy, fluorescence microscopy, nanobiotechnology, single-molecule analysis, single-cell analysis, virus, cell surface receptor, cell interaction, glycoprotein, virus-host interaction, force-distance curve, FD curve, FD-based AFM, confocal microscopy, rabies virus, receptor-ligand bonds, binding steps, free-energy landscape, membrane receptor, cell membrane, mammalian cells, MDCK cells, tip functionalization, enveloped virus, lentiviral transduction, TVA receptor, PEG linker, dynamic force spectroscopy, loading rate, EnvA glycoprotein, rupture force.

1. Introduction

1.1 Virus-cell interactions

Viruses are small and simple parasitic agents that cannot reproduce themselves. Because of their simplicity, they strictly depend on a host organism in nearly all steps of the infection cycle. Through the evolution viruses acquired the relevant molecular "passwords" or "entrance tickets" enabling to control and hijack cellular functions [1]. Consequently, nearly all viruses are species-specific and only infect a narrow range of organisms.

The infection pathway of a virus particle from its binding to the cell surface, its entry into the cytosol and the delivery of their genetic cargo within the nucleus consists of a series of consecutive steps tightly regulated [1]. The first step starts with the virus landing or "touchdown" on the cell surface *via* interactions, whether specific or not, between virion-exposed proteins and cell surface glycoproteins. These preliminary interactions are then followed by the engagement of specific receptors. These first interactions already define the consecutive complex series of processes to which viruses have to face to gain access to the intracellular compartment [2]. Such processes include virus uptake, intracellular trafficking and finally, penetration to the cytosol. Tremendous effort has been made to characterize the cellular receptors and entry pathways [3], but the molecular details by which these interactions determine cellular binding and uptake are poorly understood because of the lack of suitable technique that allows to gain information on the molecular interactions that occur at the single virus-receptor level. The understanding and exploration of the first steps of receptor-mediated endocytosis of viruses, from receptor binding to the physical internalization of the viral particle into host cells and their dynamics, is an important challenge in virology. A full picture of these interactions would provide insights valuable to medicine, cell biology, molecular biology, neurobiology, structural biology, biochemistry, biophysics, and offers novel potential therapeutic strategies [4-6].

1.2 Current methods to study virus binding to cell surface receptors

In the context of virus host interactions, the cell imposes multiple barriers to the virus entry. However, viruses exploit fundamental cellular processes to gain entry to the cell and deliver their genetic cargo. Virus entry is largely defined by the first interactions that take place at the cell surface. These first

interactions determine the mechanism of virus attachment to the cell surface, the penetration of the virus and ultimately the penetration to the cytosol. Methods to study viral infection, especially virus binding, have undergone rapid development over the last decade, in particular since viruses can be propagated and purified. It now becomes easier to obtain purified viruses for studies using biochemical and biophysical techniques [7-9]. Among the well-established methods, most of the techniques rely mainly on ensemble studies that give an average response of a population of virions, failing to account for biological variability or on methods that do not preserve the physiological sate of the cells or the virus (performed either on fixed cells or with isolated receptors). Moreover, most of the methods developed so far are based on binding assays with long incubation periods, thus lacking time-resolution to decipher the dynamical character of the first binding steps. As an example, solid-phase binding assays (**Figure 1a**) are used to measure or screen virus binding to a variety of receptor molecules such as glycan moieties [10], in which the investigated receptor is coupled to a flat surface and is allowed to interact with intact viruses [11]. Thermodynamic properties of virus-receptor binding can be obtained using surface plasmon resonance (SPR) (**Figure 1b**) [12,13]. SPR consists in flushing receptor molecules into a chamber, where they interact with a gold-coated sensor chip. Subsequent flushing of the virus into this chamber allows determining association and dissociation kinetics. The main limitation about these methods are the poor control of ligand density and orientation, which presumably affects binding [14]. More importantly, an error in SPR can arise from the multivalency of the interaction leading to underestimation of the dissociation rate due to the local high-concentration of ligand on the viral surface. Recently, microscale thermophoresis (MST) (**Figure 1c**) was applied to the study of receptor-virus interactions[15]. Besides the advantage that binding and unbinding kinetics can be measured in solution under defined and controlled conditions, this method requires a complex environment of a 3D host cell plasma membrane, with the receptors of interest incorporated. This could give rise to difficulties in isolating the effect of specific molecules. Also radioactive labeling of structural viral components and electron microscopy (EM) of infected cells have been used to investigate virus binding [16,17]. Even though EM techniques are able to give visual insights into virus entry and even spectacular three-dimensional images of the samples, the identification of cellular factors and pathways involved in the uptake process is difficult. Moreover, to characterize virus-

binding to cells by EM usually requires high virus concentrations and can only be operated under vacuum, which does not reflect physiological conditions and lacks dynamics.

For these reasons, compared to conventional ensemble methods, single-molecule experiments offer distinct advantages. First, conducting many sequential measurements enables to determine the distribution of molecular properties of inhomogeneous systems. Second, being direct records of the fluctuations of the system, single-molecule trajectories provide dynamic and statistical information, which are often hidden in ensemble-averaged results. Finally, they permit real-time observation of rarely populated transients, which are difficultly captured using conventional methods [18,19]. Atomic force microscopy (AFM)-based single molecule force spectroscopy (SMFS) (**Figure 1d**) and optical tweezers (**Figure 1e**) provide powerful tools to measure forces with single molecule resolution and high-temporal resolution [20,21]. Well-developed, specific grafting protocols allow the attachment of single viral particles on AFM cantilevers or beads [22,23]. Such types of measurements allow characterizing the binding of intact viruses on living cells that are kept close to physiological conditions, and has been used on a variety of viruses in the past [22,23,9,24,25]. However, assignment of forces to their corresponding molecular interactions remains difficult by using these techniques. An appropriate method would be the use of mutant virions, lacking individual glycoproteins or, in addition to single molecule measurements, employing (force-probe) molecular dynamics (MD) simulation where interactions between all atoms within a given system are calculated [22].

FIGURE 1

1.3 Atomic force microscopy

Since its invention by Binnig *et al.* in 1986 [26], the AFM has become a powerful tool in biology, physics, chemistry and medicine. Being a multi-versatile imaging platform, it enables the visualization and manipulation of biological samples, from single molecules to living cells with sub-nanometer lateral resolution and under quasi-physiological conditions [27-31]. In addition to high-resolution imaging, the high sensitivity of force measurements allows the determination of inter- and intra-molecular forces (piconewton (pN) – range) at the single molecule level [32]. Moreover, data obtained from force spectroscopy include physical parameters (*e.g.* stiffness, friction, elasticity) not measurable

114 by other methods and opens new perspectives in exploring the regulation of the dynamics of biological
115 processes [33]. It can also capture dynamic features of individual molecules in the millisecond time
116 scale [34]. The proof-of-principle stage of the pioneering experiments has already evolved into
117 established methods for exploring kinetic and structural details of interactions and molecular
118 recognition processes.
119 Compared to conventional ensemble methods, single-molecule experiments offer several advantages
120 as already mentioned in the section before [18,19]. AFM has successfully complemented electron
121 microscopy and X-ray diffraction studies of viruses [35]. Moreover, force spectroscopy measurements
122 have been used to study the mechanics between viral envelope proteins and host cell receptors at the
123 single molecule level in living cells [24,22,9,36]. Taken together, the unique flexibility of AFM to
124 image, probe and manipulate materials and biological systems (under quasi-physiological conditions)
125 [31] made it a highly versatile instrument in nanoscience and nanotechnology as well as biology, and
126 stimulated numerous discoveries and technologies [37]. Thus, it makes it an optimal tool to explore
127 the mechanisms by which virus-cell surface receptor bonds are formed as a starting point of cell entry
128 and which properties they possess in vivo. This being so, the specific binding of a particular virus to
129 cell surface receptors should be best characterized by the lifetime, affinity and free-energy of the
130 virus-receptor bonds. While AFM alone is an appropriate quantitative method to characterize binding
131 properties, it lacks the capacity to identify host cell receptors. In this context, light microscopy has
132 been a standard tool in cell biology for decades but bringing both techniques together in a sealed
133 physical environment remained difficult for a long time. To address this challenge, we recently
134 introduced the combination of FD-based AFM [28] and confocal microscopy under cell culture
135 conditions to simultaneously image animal cells and topographically map the specific binding events
136 of single viruses [36,38].

137 **1.3.1 AFM imaging of viral particles and living cells**

138 In conventional AFM imaging mode, a sharp tip placed at the free end of a cantilever contours the
139 sample surface and generates a 3D image. Different operating modes allow to image biological
140 samples. In contact mode, topographic images of biological specimens are obtained by maintaining the
141 tip in contact with the sample [39-44]. Changes in the cantilever deflection are monitored and kept

constant using an electronic feedback loop [45,46]. The image consists of the calibrated height information about the sample relief. However, contact-mode imaging turned out to be less suitable for weakly attached and soft samples, as bio-molecules are often pushed away or get damaged by the AFM stylus during imaging [47]. To overcome this disadvantage, dynamic force microscopy (DFM, originally termed tapping or oscillation mode) was invented to minimize the friction and the force applied between tip and sample [48]. In its simplest application, the cantilever is oscillated close to its resonance frequency as it raster-scans over the surface and touches the sample only at the end of its downward movement, resulting in amplitude reductions at positions of elevated objects. The reduction in oscillation amplitude is used as the feedback-control signal to measure the surface topography. As the lateral forces are greatly reduced during imaging, the study of biological specimens has therefore exceptionally benefited from the development of DFM and has been applied to a variety of biological objects that are only weakly adsorbed to supports [48-51] or are highly corrugated, such as living cells [52].

With AFM, virus particles can be visualized in appropriate buffers and at room temperature [53-56]. Most importantly, AFM yields three-dimensional images and does not rely on symmetry averaging. In contrast to EM, the resolution of AFM is very good in the vertical direction (less than a nanometer). AFM has been utilized to study various viruses and their substructures by topographical imaging [57], their mechanical properties [58-60] and human immunodeficiency virions were imaged on lymphocytes at high resolution and considerable details of the process of virus-cell attachment were obtained [61].

Living mammalian cells are very fragile and complex systems protected from the external environment by a highly dynamic and flexible barrier, called the plasma membrane. This very sophisticated structure contains a wide variety of biomolecules (carbohydrates, glycoproteins,…), and plays key roles in fundamental cellular processes, such as signaling, communication, adhesion and sensing. Depending on the physiological cell state, the structural and functional assembly of cellular surfaces can be adapted, changing dynamically its chemical and biophysical properties [62]. Therefore, cellular structures should be investigated close to their native state. High-resolution

169 imaging of cellular surfaces usually require fixed or frozen cells, failing in probing the dynamic
170 character of the molecular events occurring at the plasma membrane (*e.g.* cryoelectron microscopy
171 [63]) or to specifically label the studied molecules with fluorophores (*e.g.* far field optical nanoscopy
172 methods [64]). Nowadays, AFM provides a powerful tool to image the surface architecture of living
173 cells with a nanometric precision, in real time and under physiologically relevant conditions [65].
174 AFM has been successfully applied to gain insights into the surface morphology of microbes such as
175 bacteria [66], fungi [67] or yeasts [68] with a resolution up to 10 nm [69]. Dynamic functional cellular
176 processes were also observed using AFM imaging, such as bacterial pore germination [70] and cell
177 division [71].

178 **1.3.2 Single molecule/ virus force spectroscopy**

179 The AFM can be used not only to image but also to manipulate biological samples. In the so-called
180 SMFS (single-molecule force spectroscopy) mode, the AFM tip is approached and retracted from the
181 sample while recording a force-distance (FD) curve (**Figure 2a**). From the approach curve, structural
182 height, surface forces and mechanical deformation of the sample can be quantified, whereas from the
183 retraction curve the elastic modulus, dissipation and adhesion can be extracted [72]. A tip
184 functionalized with a certain molecule (*e.g.* lectin, antibody or virus) is upgraded to a biosensor able to
185 measure specific interaction forces between the tip-linked molecule and cell surface receptors [73-75].
186 The interaction (unbinding) force is measured by following the deflection of the cantilever, which
187 behaves like a Hookean's spring, where the force F exerted on the sample by the AFM tip scales
188 linearly with the cantilever deflection Δz, according to Hooke's law:

$$F = -k_c \cdot \Delta z$$

189 In this equation, k_c refers to the cantilever's spring constant and Δz to the deflection. By pulling the
190 AFM tip away from the surface, an increasing force is applied onto the receptor-ligand complex until
191 the pair dissociates. For a detailed protocol describing the application of single-molecule force
192 spectroscopy on living cells please refer to Puntheeranurak et al. [76].

193 However, because rupture forces observed between a tip-linked ligand and cell surface receptors
194 depend on the rate at which force load on the bond is applied, the quantification of forces is relative
195 [77]. In combination with theoretical models, probing the force dependency on the loading rate

196 enables the receptor-ligand's free energy landscape to be determined and the quantification of unique
197 structural, kinetic and energetic parameters of viruses interacting with cell surface receptors (**Figure**
198 **2b,c**) [78]. In the past, SMFS measurements have been used to study the mechanics between viral
199 envelope proteins and host cell receptors at the single molecule level in living cells [24,22,9,36],
200 which are presented and explained in great detail in section 1.3.3.
201 Another mode, which combines AFM imaging and SMFS, is called FD-based AFM, were each FD
202 curve records a local stochastic unbinding event from which these properties can be inferred and
203 directly mapped to the sample topography as FD curves are obtained at each pixel on the sample
204 surface (**Figure 2a**). Just very recently, two important limitations related to the lateral and temporal
205 resolution were circumvented, allowing the imaging and force probing of biological samples with high
206 lateral (~50-100 nm) and temporal resolution (~ms per FD curve) [28,79,80]. The latter will be
207 described in detail in section 1.3.4, as this mode is the most reliable and best way to study virus
208 binding sites quantitatively on living cells.

209 **FIGURE 2**

210 Reconstruction of the binding free-energy landscape can be obtained using appropriate biophysical
211 models giving access to the kinetic and thermodynamic parameters of biomolecular interactions. To
212 this end, we need to relate how measurements performed out-of-equilibrium can give access to the
213 equilibrium free-energy and kinetic parameters. The first phenomenological description of how an
214 external force pulling on a bond reduces the activation energy barrier towards dissociation was
215 described by Bell in a seminal article on cell adhesion (**Figure 2c**) [81]. This description was latter
216 formulated by Evans and Ritchie [78]. Focused on the bond dissociation kinetics, the Bell-Evans
217 model predicts that the force of a single energy barrier in the thermally activated regime linearly
218 increases with the logarithm of the force loading rate, F ~ln (LR) (**Figure 2b**) [78]. A rigorous
219 theoretical framework for the estimation of thermodynamic parameters is provided by fluctuation
220 theorems such as the Jarzynski Equality (JE) and its generalization, the Crooks fluctuation theorem
221 [82]. Previous studies have shown that the free-energy difference between initial and final equilibrium
222 states could be calculated *via* a non-equilibrium, irreversible process that connects them, thus bridging

223 the gap between equilibrium and non-equilibrium statistical mechanics [82]. A more recent theoretical
224 approach, the Friddle-Noy-de Yoreo (FNdY) model describes the force spectrum of a ligand-receptor
225 bond attached to a force transducer, consisting in two primary regimes. First, at low loading rate, a
226 close-to-equilibrium regime exists, where rebinding events can occur, that is characterized by an
227 equilibrium force, F_{eq}. At higher loading rate, a kinetic regime characterized by a fast non-equilibrium
228 bond rupture is described [83]. The F_{eq} defines the equilibrium force for the bond-transducer system:

$$F_{eq} = \sqrt{2k_{eff}\Delta G_{bu}}$$

229 The mean rupture force is defined as:

$$\langle F \rangle = F_{eq} + F_{\beta} \ln\left(1 + e^{-\gamma} R\left(F_{eq}\right)\right)$$

230 with

231 $$F_{\beta} = \frac{k_B T}{x_{\beta}} \qquad \text{and} \qquad R\left(F_{eq}\right) = \frac{L_R}{k_{off}(F_{eq}) F_{\beta}} \ .$$

232 F_{β} is the thermal force, γ the Euler's constant, k_BT the thermal energy, k_{eff} the effective spring constant
233 of the transducer, ΔG_{bu} is the equilibrium free-energy between the bound and unbound state and
234 $k_{off}(F_{eq})$ the unbinding rate scaled by the Boltzmann-weighted energy of a spring extended between the
235 barrier location and the relative displacement of the spring minimum under F_{eq} (for further details see
236 [83]).

237 **1.3.3 Previous studies of virus interactions with purified receptors and cells using AFM**

238 Virus-host cell surface interactions mark the first critical step of infection. Hence, forces involved in
239 this process are essential. AFM based single-virus force spectroscopy (SVFS), whether combined with
240 imaging or not, has become a robust, accurate and reliable technique within the past decade. It has
241 been applied to study virus interactions with purified receptors and on cells. A few selected examples
242 of SMFS studies are described here in more detail and a summary can be found in Table 1 although
243 the authors raise no claim to completeness.

244 Rankl et al. [23] showed that human rhinovirus (HRV) forms multiple parallel interactions with living
245 host cells utilizing AFM-based SVFS. Moreover, the binding forces were confirmed by in vitro
246 experiments on artificial receptor surfaces and an estimation of the number of receptors involved in

247 binding were extracted. Furthermore, estimation of k_{on}/k_{off} describing the kinetics of the interaction
248 between HRV2 and plasma membrane-anchored receptors were obtained. In another application of
249 SVFS the variability of single molecule interactions for influenza virus was studied using AFM
250 measurements on different living host cell types [22]. Using various cell types that differ with respect
251 to their sialic acid surface composition, the study revealed that hemagglutinin (HA, viral envelope
252 spike protein) receptor specificity might not be a direct indicator for binding to living cells. Moreover,
253 sequential unbinding events were observed with each individual event following a unique unbinding
254 trajectory with different kinetic and thermodynamic parameters. Also for HIV-1 (human
255 immunodeficiency virus type 1), the interaction of the spike protein with co-receptors was studied
256 using SVFS. It has been shown that engagement with the primary receptor CD4 is very stable but only
257 for a short lifetime until the viral glycoprotein gp120, organized with gp41 in a homotrimeric
258 complex, finds its co-receptor molecule [25]. More recently, Alsteens et al. [36] introduced an AFM-
259 confocal microscopy set-up that allows imaging cell surfaces and simultaneously probing virus
260 binding events within the first millisecond of contact. Moreover, they present theoretical approaches to
261 contour the free-energy landscape of early binding events between an engineered virus (rabies virus,
262 RABV) and cell surface receptors.

263 **Table 1:** Overview of SVFS studies on purified receptors and/ or living cells in the years 2005–2017
264 (no claim to completeness)

Virus	**Purified receptors, (living) cells, membranes, etc.**	**Study**	**Author, Year, Reference**
Vesicular stomatitis virus (VSV)	Membranes of different phospho-lipid compositions	Carneiro *et al*. studied the interactions between VSV and phosphatidylserine and found out that binding forces dramatically depend on the membrane phospholipid composition.	Carneiro et al., 2005, [84]
HIV-1	Receptor expressing cells	Monitoring of early fusion dynamics of HIV-1 at single virus level.	Dobrowsky et al., 2008, [25]
Human Rhinovirus	- Very low-density lipoprotein receptor (VLDLR) - Cells expressing LDLR	Discovery of multiple receptors involved in human rhinovirus attachment to living cells and comparison to experiments on purified receptor surfaces.	Rankl et al., 2008, [23]
Tobacco mosaic virus		They show the possibility to study nucleic acid – protein interactions in more	Liu et al., 2010, [85]

		complicated systems using SVFS on Tobacco mosaic virus, where they investigate RNA-coat protein interactions by pulling genetic RNA step by step out of the virus.	
Influenza virus	Different types of living cells	Sieben *et al.* showed that Influenza virus binds its host cell using multiple dynamic interactions.	Sieben et al., 2012, [22]
- Vaccina virus - Influenza virus - Bacterio-phage AP22	- Erythrocyte monolayer - Bacterial film of phage-sensitive *Acinetobacter baumannii*	They show that it is of great importance in terms of reliability of the results to verify the presence of the virus particle attached to the tip by complementary methods such as electron microscopy and/ or dielectrophoresis.	Korneev et al., 2016, [86]
Influenza A virus (H1N1)	- CHO cells - Human alveolar basal epithelial cells	This group used SVFS as a supporting technique to genetically characterize an adapted pandemic 2009 H1N1 influenza virus that reveals improved replication rates in human lung epithelial cells.	Wörmann et al., 2016, [87]
Pseudotyped rabies virus	Living MDCK cells expressing receptor for virus binding	Alsteens *et al.* introduced an advanced AFM probing technique in combination with optical microscopy to nanomechanically map the first binding steps of a virus to animal cells.	Alsteens et al., 2017, [36]

SVFS enables to decipher the role of individual viral constituents during their very first interactions with target cells. Furthermore, the time-scale of force spectroscopy experiments allows gaining insights into the dynamics of the molecular processes involved in virus-receptor interactions and virus internalization. Overall, this innovative method addresses the molecular mechanism of virus binding with high spatial and high temporal resolution and moreover provides quantitative insights into the kinetics and thermodynamics of individual binding steps.

1.3.4 Multiparametric imaging and quantitative mapping of virus binding sites

For a long time, AFM investigations of cellular processes have been limited by their poor spatial and temporal resolution. In addition, AFM imaging of mammalian cells is still a challenging task, as cell surface components can be easily deformed and damaged by the vertical and lateral forces applied by the scanning probe. Therefore, FD-based AFM methods that vertically oscillate the cantilever in the kilohertz range on top of the sample have been developed. Recording FD curves at frequencies much

278 lower than the resonant frequency of the cantilever allows precise control of the applied force in the
279 piconewton range [88] with a high positional accuracy. Thereby, cellular membranes can be imaged at
280 high spatial resolution while probing dynamic molecular events occurring in the millisecond range.
281 Furthermore, the reduced contact time between the AFM tip and the sample (~ ms) limits damaging
282 lateral forces on the examined structures, yielding topographs of cell surfaces closer to their native
283 state.
284 Using FD-based AFM, the interactions occurring between viruses and their receptors on the plasma
285 membrane can be studied directly on living cells. Using AFM tips functionalized with a single viral
286 particle, the surface of living cells can be imaged while recording virus adhesion events
287 simultaneously. Both topography and adhesion parameters extracted from each point of the probed
288 surface can be displayed in correlated maps with high resolution. This allows locating and evaluating
289 the number and density of cell surface receptors that interact with the single viral particle.
290 Furthermore, a FD curve can be displayed from each pixel of the recorded maps, so that FD curves
291 corresponding to virus binding events can be extracted for further DFS analysis. Thereby, kinetic and
292 thermodynamic parameters governing the complex virus-receptor interactions in close-to-
293 physiological conditions can be extracted. As the attachment of viral particles to cellular surfaces is
294 usually a multistep process involving multiple glycoprotein-receptor binding events, this method
295 allows to gain insights into the mechanistic processes involved in the initial events of viral infection.
296 By combining this approach with the tools of genetic engineering, the individual role of viral
297 glycoproteins can be deciphered using mutant viruses deficient in various glycoprotein expression.
298 This provides indications on how viruses modulate and optimize their attachment to cellular surfaces
299 to efficiently gain access to the cytoplasm.

300 # 2. Materials

301 ## 2.1 Viruses, cell lines and reagents

302 - Phosphate-buffered saline (PBS) buffer.
303 - Virus solution: suspension of virions in buffer (e.g. PBS) (~10^8 PFU mL^{-1}).

304 - Animal cell lines for cell culture (e.g. MDCK or CHO cells) expressing and non-expressing
305 the receptor of interest.
306 - Cell culture medium: buffer (e.g. Dulbecco's modified Eagle medium with 4500 mg/L
307 glucose, L-glutamine, sodium pyruvate and sodium bicarbonate), 10 % serum (e.g. fetal
308 bovine serum, sterile filtered), antibiotics (e.g. 100 units mL^{-1} penicillin and 100 µg mL^{-1}
309 streptomycin).
310 - Trypsin.
311 - Dulbecco's Phosphate-Buffered Saline (DPBS) buffer.

312 **2.2 Equipments**

313 - Atomic force microscope with required capabilities (e.g. Bioscope Catalyst or Bioscope
314 Resolve (Bruker Nano, Santa Barbara, CA) with PeakForce QNM mode).
315 - Inverted optical microscope (Observer Z1, Zeiss, Germany) equipped with epifluorescence or
316 confocal microscopy (LSM800, Zeiss, Germany)
317 - Upright bench top microscope for examining probes (e.g. Stemi DV4, Zeiss or equivalent)
318 - Si_3N_4 cantilevers with spring constants of ~0.08 N/m (e.g. PeakForce QNM- Live Cell
319 (PFQNM-LC), Bruker Nano, Santa Barabara, CA).
320 - Active vibration isolation table (TS 150, HWL Scientific Instruments GmbH, Germany).
321 - Acoustic enclosure for the AFM and inverted optical microscope with thermo regulation at 35
322 ± 1°C.
323 - Silicon hollow fiber membrane module (PDMSXA-2500 cm^2, PermSelect, MedArray, Ann
324 Arbor, MI).
325 - Synthetic air supplemented with 5% CO_2 gas bottle.
326 - Pressure-reducing regulator with flow rate control (0.1 - 1 l/min) (Swiss Opto varius, Gloor,
327 Switzerland).
328 - Resin tubing (Cole-Palmer).
329 - Glass-bottom Petri dishes.
330 - Sofware for FD curve analysis (e.g. Nanoscope software (Nanscope 9.3R1; Bruker)).

331

332 **2.3 Chemicals for tip functionalization**

333 - Ethanolamine hydrochloride ($H_2NC_2H_4OH$)

334 - Dimethylsulfoxide anhydrous (> 99.9% $(CH_3)_2SO$)

335 - Molecular sieves, 3 Å (beads, 8-12 mesh)

336 - Heterobifunctional crosslinker (e.g. NHS-PEG_{27}-acetal provided by H. Gruber, JKU, Linz,

337 Austria).

338 - Triethylamine (> 99.5% $(C_2H_5)_3N$)

339 - Sodium cyanoborohydride ($NaCNBH_3$)

340 - Citric acid

341 - Chloroform (> 99.9% $CHCl_3$)

342 - Ethanol absolute, G Chromasolv (> 99.9% C_2H_5OH)

343 - Milli-Q water (Millipore)

344 - Acidic piranha solution (70% sulfuric acid, 30% oxygen peroxide)

345

346 # 3. Methods

347 **3.1 Virus production, cell culture and sample preparation**

348 To ensure successful functionalization of AFM tips, a highly pure virus solution is required. This
349 ensures a solution of viral particles that is free from cellular aggregates or macromolecules that would
350 adsorb to the AFM probe. This tip contamination can modify the shape of FD curves and alter the
351 topography images by lowering the resolution and introducing imaging artefacts [28]. To reach a high
352 purity of viral solutions, ultracentrifugation through sucrose, cesium chloride, iodixanol and/or
353 potassium tartrate density gradients is often used [89,90]. Amplified virions should be suspended in
354 buffer solution (*e.g.* PBS) and used as such for tip functionalization (see 3.2). Depending on the size of
355 virions and the tip radius of curvature, concentrations around $\sim 10^7$-10^{10} plaque-forming units
356 (PFU)/mL should be used.

357 Animal cell lines are typically grown in Dulbecco's modified Eagle medium supplemented with serum
358 and antibiotics within cell culture flasks at 37°C in a humidified, 5% CO_2-supplemented atmosphere.
359 Regular cell passages are performed by detaching confluent monolayers of cells from the bottom of
360 the flask using trypsin and seeding them in a less concentrated fashion. Before AFM measurements,
361 the last cell passage should be performed between one and three days before the experiment,
362 depending on the rate at which the cells grow. Cells are seeded in a glass bottom Petri dish in an
363 adequate concentration to reach confluence on the day when the experiment is planned. Cells should
364 be well adhered on the surface and form a continuous monolayer.

365 **3.2 Tip selection and functionalization**

366 AFM imaging or force spectroscopy of biological samples or interacting partners respectively require
367 cantilevers with a small spring constant (k_c ~0.01-0.1 N m^{-1}) in order to achieve high lateral resolution
368 and to measure adequately forces arising from interactions between single biomolecules (F ~5-250
369 pN) [27]. In addition, for the tip to precisely follow the vertical movement applied by the piezoelectric
370 scanner, the resonance frequency of the cantilever has to be at least 5 times higher than the frequency
371 at which the probe is oscillated to record FD curves [80]. Since the detection of fast and dynamic
372 biomolecular interactions require to oscillate the probe in the kilohertz range, cantilevers with high
373 resonance frequencies (> 100 kHz) are utilized [91]. Furthermore, due to the complexity of the
374 structure of cellular samples, specially designed probes (e.g. PeakForce QNM-Live Cell probes (PF-
375 LC), Bruker) are used to image living cells [88]. Usually, height differences between adjacent cells
376 causes imaging problems because AFM probes have a tip height below 5 µm. This leads to shadowing
377 and blind spots in the images where the tip was not able to reach the surface and the cantilever comes
378 into contact with the cell body. Specially designed tips with height ~17 µm enable to image cell
379 surfaces with large height differences. The high resolution is maintained thanks to a protruding area at
380 the tip apex, displaying a radius of curvature of ~ 65 nm.

381 In the past decade, a lot of progress has been made in developing and optimizing coupling strategies
382 for single molecule force spectroscopy [92]. The most common functionalization method is tethering
383 the virus on an AFM tip in a multiple-step crosslinking procedure, including the creation of reactive

384 amino groups on the chemically inert tip surface [93], followed by the covalent binding of the cross-
385 linker (with different lengths) and finally coupling of the sensor molecule. The inert water soluble
386 PEG-cross linker is designed hetero-bifunctional [94] with one end being an N-hydroxysuccinimide
387 (NHS) group to bind free amino groups on the AFM tip and the other end specifically designed to
388 react with the desired virus for coupling (**Figure 3**). Since lysine residues (amino acid with a pending
389 NH_2 group) are abundant in most of the glycoproteins of virus surfaces, the acetal-PEG_{27}-NHS linker
390 for virus coupling is utilized [92].
391 To create reactive amino groups, AFM tips are immersed in chloroform for 10 min, rinsed with
392 ethanol, dried with a stream of filtered argon, cleaned for 10 min in an ultraviolet radiation and ozone
393 (UV-O) cleaner (Jetlight), and immersed overnight in an ethanolamine solution (3.3 g of ethanolamine
394 hydrochloride in 6.6 mL of DMSO). The cantilevers are then washed three times with DMSO (3 x
395 1min), followed by three times in ethanol (3 x 1 min) and dried with argon. The cantilevers can be
396 stored under argon for up to 3 weeks (preferably < 1 week), if they are not used immediately.
397 To reduce the grafting density of the linker on the AFM tip, 1 mg of acetal-PEG_{27}-NHS is diluted in
398 0.5 mL chloroform with 30 µL trimethylamine (TEA). Ethanolamine-coated cantilevers are immersed
399 for 2 h in this solution, then washed three times with chloroform (3 x 10 min) and dried with argon.
400 Also here, the cantilevers can be stored under argon for up to several months, if they are not used
401 immediately.
402 For coupling the virus to the free amino end of the PEG linker, the cantilevers are immersed for 10
403 min in 1% (w/v) citric acid in water and washed three times with milliQ water (3 x 5 min) and dried
404 with argon. An ~ 80 µL aliquot of the virus solution can be thawed and centrifuged at 1,677 g for 5
405 min to remove aggregates if necessary. As well as removing aggregates, this gentle centrifugation
406 ensures that the remaining virus solution is highly diluted, as is required to bind only a few viruses to
407 the functionalized AFM tip. Next, an 80 µL volume of virus solution is pipetted onto the tips (placed
408 in a radial manner with the tips oriented in the center) on Parafilm (Bemis NA) in a small polystyrene
409 dish stored within an ice box. A freshly prepared solution of $NaCNBH_3$ (2 µL, ~6 wt% in 0.1 M
410 NaOH(aq)) is gently mixed into the virus solution and the cantilever chips gently positioned with their
411 cantilevers extending into the virus drop. The ice box is incubated at 4 °C for 1 h before being

412 removed and 5 µL of 1 M ethanolamine solution (pH 8) gently mixed into the drop to quench the
413 reaction. The icebox is incubated for a further 10 min at 4 °C, the cantilever chips are removed,
414 washed once in ice-cold PBS or any other buffer, and stored in individual wells of a multiwell dish
415 containing 2 mL of ice-cold buffer per well until used in AFM experiments. During these
416 functionalization steps the virus-functionalized cantilevers are never allowed to dry. Transfer of the
417 functionalized AFM cantilevers to the buffer and then to the AFM should be done rapidly (≤20 s), and
418 during transfer a drop of PBS buffer should always remain on the cantilever and tip. Cantilevers are
419 used in AFM experiments the same day as being functionalized with the virus.
420 An elegant way to control the successful grafting of a viral particle at the apex of the AFM tip is to
421 record confocal microscopy images of the tip functionalized with a fluorescently tagged virus [36].
422 Alternatively, scanning electron microscopy (SEM) images of the probe can be taken to visualize
423 virions at the tip apexes. However this is more challenging, as it requires to dehydrate the sample
424 without destroying the delicate tips to allow SEM imaging in vacuum. This can be performed through
425 immersing the tips in graded ethanol baths (e.g. 30, 50, 75, 90, 100 % for 10 minutes each) [36].
426
427
428 **3.3 AFM imaging and probing of biophysical properties on live cells**
429 Measuring interactions between functionalized tips and cellular membranes can lead to the detection
430 of non-specific adhesion events with other cell surface molecules. Therefore, as an internal control,
431 cells containing the endogenous receptor should be mixed with cells lacking the receptor of interest
432 enabling direct comparison. To this end, different cell types are fluorescently labeled (**Figure 3**).
433 **FIGURE 3**
434
435 Cells from the two cell lines should be mixed after splitting, seeded together in a glass-bottomed dish
436 and cultured in cell culture conditions (37°C, 5% CO_2, 95% RH) in order to reach confluency on the
437 day of the AFM experiment. A dish is then transferred to the AFM heated at 37°C. To generate a 95%
438 relative humidity atmosphere of 5% CO_2 in air, the gas mixture is blown through the silicon hollow

439 fiber membrane filled with MilliQ water at a flow rate of 0.1 L/min. Next, the functionalized AFM tip
440 is mounted into the cantilever holder and placed in the optical head. The laser spot is then aligned at
441 the free end of the cantilever (in some set-ups, this can be done prior to mount the AFM head on the
442 microscope) and the sum into the photodetector is maximized (see **Note 1**). The system should then be
443 left for ~15 min to equilibrate, until the signal into the photodiode is relatively stable, indicating a low
444 thermal drift [80].

445 The first step of AFM measurements is the calibration of the force transducer and optical detection
446 pathways that will be used for imaging and nanomechanical mapping. For quantitative measurements,
447 the output data from the AFM device have to be treated adequately, in order to accurately extract the
448 force exerted between the tip and the sample. First, the sensitivity factor of the optical detection
449 system has to be determined. It relates the voltage output of the photodiode and the deflection of the
450 cantilever. The sensitivity factor (nm V^{-1}) can be determined from the tangent of the approach curve of
451 the tip on a rigid substrate on which the sample vertical displacement is equal to the cantilever vertical
452 deflection. The software can thereby determine the cantilever deflection required to generate a certain
453 voltage difference into the position-sensitive photodiode. Second, the spring constant of the cantilever
454 has to be determined, to allow determining the force acting on the probe from the cantilever deflection.
455 The nominal spring constant of cantilevers estimated from the dimensions and materials mechanical
456 properties that is furnished by manufacturers for a batch of probes may differ significantly from the
457 actual individual k_c value. To accurately relate the cantilever deflection to the force acting on the tip,
458 the spring constant of each cantilever has to be determined experimentally [20]. The most commonly
459 used method is based on relating the average energy of thermal vibrations of the cantilever with the
460 absolute temperature of the system using the equipartition theorem [95-97]. This so-called thermal
461 noise (or thermal tune) method is implemented in many commercial atomic force microscopes and is
462 applicable for the calibration of cantilevers in liquid. It was however shown that the error in
463 determining the spring constant of cantilevers can be as high as 20% [98], with large user-dependent
464 variations in the calibration of the same cantilevers [99]. Therefore, some manufacturers provide AFM
465 probes that are individually precalibrated using laser Doppler vibrometry, providing more accurate

466 values for cantilever spring constants [100]. This allows performing a 'no touch' calibration of the
467 deflection sensitivity of the cantilever. This method is preferable for virus-derivatized probes, to avoid
468 pressing the cantilever on a hard surface, which could damage the functionalized tip. To do so, the pre-
469 calculated value of the cantilever spring constant is introduced into the software, and thermal tune
470 (which is done at a position where the tip is removed at least 100 µm from the sample surface) is
471 performed to calculate the deflection sensitivity.

472 At this point, a fluorescence image should be taken, to allow distinguishing the different cell types on
473 the monolayer. The AFM tip can then be approached on top of the area of interest and brought in
474 contact with the cell surface, using parameters minimizing the force (<500 pN) applied by the probe
475 during the first contact (see **Note 2**) (**Figure 4a,b,c**). Well-defined images are best taken on cells that
476 form a relatively flat monolayer. The recorded image should contain at least two cells (one expressing
477 the receptor of interest and one lacking the receptor) (see **Note 3**) to facilitate comparison of adhesion
478 events and other biophysical properties (**Figure 4d,e**). Then, imaging parameters have to be optimized
479 in order to extract high-resolution topographs and adequate FD curves for subsequent analysis. These
480 parameters can change depending on the tip and sample used and are mainly fine-tuned by a trial-and-
481 error process guided by the shape of the displayed FD curves. The latter should exhibit a low noise
482 level, a flat baseline (from the contact point) and a low hysteresis between the approach and retract
483 curves. Extracted topography data should be similar from both trace and retrace scanning lines. Here
484 are a few indications on fundamental parameters that can be tuned, together with typical value ranges
485 used for animal cell imaging.

486 - The maximum force applied is the imaging setpoint that is used as a feedback for the movement of
487 the piezoelectric scanner. This force should be low enough to limit damages on cell surfaces, but
488 sufficient to allow tip-linked virions to reach the plasma membrane and interact with cellular
489 receptors. Typically, imaging forces around 300-500 pN are used, depending on the cell type,
490 properties and shape.

491 - The oscillation frequency determines the number of approach-retraction cycles exerted by the AFM
492 probe in a period of time and thus defines the contact time of tip-bound particles with the cellular

493 surface. Using a lower frequency increases the contact time, which provides a longer time frame for
494 virus-receptor interactions to take place. As the tip-sample contact approximately occurs during one
495 fourth of a scanning cycle, oscillation frequencies of 0.125 or 0.250 kHz should be used, in order to
496 allow sufficient time (~1 ms) for virions to bind receptors adequately. The speed of the scanning
497 movement of the AFM probe should be adapted to the oscillation frequency used and be
498 approximately 2000 times less. For example, for a 256 x 256 pixels image recorded using an
499 oscillation frequency of 0.25 kHz, the scanning speed used should be 0.125 Hz.

500 - The oscillation amplitude defines the height at which the tip is retracted from the imaged surface
501 during the oscillation movement. When imaging soft and sticky samples such as cellular membranes, a
502 large amplitude (typically > 500 nm) is required to pull the probe out of contact from the cell surface.
503 Increased amplitudes induce a greater tip velocity and result in higher hydrodynamic drag. This
504 problem can be partially circumvented by using specially designed probes, with a tip height >15 µm.
505 This reduces the hydrodynamic drag force variation, since the cantilever is moved far from the sample
506 surface.

507 - Feedback gains determine how the quick the piezoelectric scanner will react to maintain the
508 maximum measured force equal to the force setpoint. Increased gains allow imaging with a high
509 resolution and accurately tracking the sample surface. Gains should therefore be increased until the
510 point where the system oscillates and then reduced to a value slightly below that point to ensure
511 maximal contrast imaging.

512 **3.4 Data processing**

513 The data extracted from the raster scanning of cell monolayers comprise a topography image of the
514 sample surface together with high amount of FD curves (e.g. 65 536 curves for a 256 x 256 pixels
515 image) that locally quantify biophysical properties and interactions between the tip-linked viral
516 particle and the plasma membrane of investigated cells (**Figure 4d**). To adequately reconstruct
517 multiparametric maps and match the measured intrinsic physical properties to the topography of the
518 sample, some off-line analysis is required to provide the software with corrected FD curves that
519 eliminate unwanted effects due to the recording conditions. To reconstitute the adhesion maps (**Figure**

520 **4d,e**), the recorded retraction curves are used, where the typical signature of adhesion events can be
521 observed. The drag force acting on the cantilever during its oscillatory movement can induce a tilt in
522 the shape of the recorded curves, that should therefore be corrected by a subtraction of a linear fit of
523 the last ~30% of the baseline region. To evaluate the specificity of adhesion events, one should take
524 into account rupture events occurring at a certain distance from the cell surface. Depending on the
525 extended length of the PEG linker when bond breakage occurs, the size and localization on the tip of
526 the attached viral particle and the mechanical properties of the cell membrane, specific binding events
527 should appear at distances between 50 and 300 nm from the sample surface (**Figure 4f,g**). When
528 investigating biological samples, defining the exact contact point between the tip and the probed
529 surface can be particularly complex, due to the high deformability of soft cells, the structural
530 heterogeneities of the surface and the long-range surface forces involved. Therefore, software analyses
531 only provide an estimate (*e.g.* by linearly extrapolating the contact region to zero force) of the first
532 contact point on FD curves that usually lead to negligible approximation errors.
533 **FIGURE 4**
534
535 To extract curves of interest from the pool of FD curves recorded, a second witness for the specificity
536 of interactions lies in the elongation pattern of the PEG linker, *i.e.* the shape of the retraction curve
537 from the contact point to the bond rupture point. Fitting this part of the curve with the worm-like chain
538 (WLC) model [101] for polymer extension ensures that the bond rupture observed corresponds to the
539 breaking of an interactions occurring between the sample surface and a species attached at the free end
540 of the PEG linker. The displayed adhesion map can then provide qualitative information on the
541 number, localization and spatial distribution of adhesion events on the probed cellular surfaces
542 (**Figure 4e**).
543 In addition, further analysis of specific FD curves allows to extract quantitative information on kinetic
544 and thermodynamic parameters of the probed interactions. To evaluate the dependency of the bond
545 rupture force on the loading rate, the adhesion force together with the loading rate have to be extracted
546 from each individual binding event. The loading rate is calculated using the slope of the force versus
547 time curve by linearly fitting at least one third of the curve just before breaking of the bond. Both

548 values can then be displayed in a DFS plot (force *vs* loading rate) (**Figure 5a**). Using typical
549 oscillation frequencies of 0.125 and 0.250 kHz, the loading rate range applied to the virus-receptor
550 bond usually varies between 10^4 and 10^7 pN s^{-1}, depending on when rupture occurs on the tip
551 trajectory and the elongation of the PEG linker at that time. Fitting the data from the DFS plot allows
552 to extract the kinetic parameters of the interaction, using appropriate models (See Section 1.3.2).
553 Different strategies can be used to probe the LR dependency of the rupture force over the whole LR
554 spectrum [102]. For example, all the data points in the DFS plot can be fitted with the best fit straight
555 line. However, this could fail to capture all the information contained in the DFS plot, such as the
556 presence of multiple interactions. An elegant way to proceed with the analysis is to separate the DFS
557 plot in ~4-8 narrow LR ranges and plot the distribution of rupture forces as histograms [36] (**Figure**
558 **5a,b**). Fitting these histograms with Gaussian distributions allows to determine the presence of single
559 or multiple peaks, corresponding to one or several parallel virus-receptor interactions (see **Note 6**). For
560 each LR range, the mean rupture force of each peak can be reported together with the corresponding
561 mean LR value in a new DFS plot. These data points can then be fitted with either a linear iterative
562 algorithm (Levenberg Marquardt) along with the Bell-Evans model (**Figure 5c,d**) [78] or a nonlinear
563 iterative algorithm (Levenberg Marquardt) along with the FNdY model (**Figure 5d**) [83], that has to
564 be used only if the forces measured do not scale linearly with the logarithm of the loading rate. An
565 extensive overview on analysis and fitting dynamic force spectroscopy (DFS) data can be found in ref.
566 [103] as well in ref. [83], while a comparison of the different models was performed by Hane *et al.*
567 [104].
568 Fitting the data with the FNdY model requires calculating the effective spring constant of the probed
569 setup (**Figure 1a**), since the finite near-equilibrium unbinding force F_{eq} depends on the stiffness of the
570 force transducer. This is equivalent to the stiffness of the whole system, i.e. the cantilever, the linker,
571 the virion and the cell surface, acting as springs in series. This value can either be extracted by fitting
572 individual force *vs* piezo movement curves or theoretically modelled [38,105,106], since each
573 individual spring behavior can be estimated using the appropriate biophysical model (e.g. worm-like
574 chain model for protein extension [101], PEG elasticity models for the linker extension [106], ...).
575 FIGURE 5

576
577 # 4. Notes

578 1. For accurate force measurements, the laser should be aligned at the free end of the cantilever and
579 correctly sent in the middle of the position-sensitive photodetector. If the laser spot cannot be
580 located close to the cantilever, there might be an air bubble trapped between the cantilever and the
581 tip holder. In this case, the AFM head should be removed from the liquid environment, and then
582 re-submerged. Alternatively, the cantilever can be removed from the holder and replaced. If the
583 sum is zero when the laser spot is correctly located on the cantilever, align the mirrors manually,
584 so that a signal from the laser is detected in the photodiode.
585 2. Engaging the probe on the cell surface is a critical step, as the tip has to come in close contact with
586 the cell membrane, without altering its shape or destroy its constituents. Therefore, the engaging
587 force setpoint should be low enough to avoid deteriorating the probed biological materials.
588 However, a too low engage setpoint can lead to a 'false engage' when the tip is too far from the
589 surface. In this case, the engaging force should be increased to ensure proper engagement.
590 3. When choosing an appropriate area for imaging, it might be difficult to find a zone were two
591 different cells (i.e. expressing and not expressing the receptor of interest) are close to each other.
592 This might be due to an imbalance between the number of cells from the two types in the
593 confluent cell layer. To overcome this issue, different ratios should be used to mix the cells before
594 seeding. It may be that one cell line grows faster than the other (generally, mutant cells divide
595 slower) yielding a confluent layer containing more cells of one type. An appropriate ratio should
596 then be found to generate a monolayer containing ~50/50 % of each cell type.
597 4. Flat and 'featureless' cells are intrinsically easier to image than round and/or rough cell surfaces
598 and should thus be chosen for imaging, based on their appearance on the optical image of the
599 sample. Cell division may however occur while imaging, during which the cells round up and
600 detach from the surface. In this case, imaging should be stopped and started again on other cells.
601 5. Adhesion maps allow to localize interactions with cellular receptors, and provide an estimate of
602 the abundance of these interactions. In some cases however, adhesion maps can look different than
603 expected. If it shows no interactions at all, it is probably because there is no viral particle grafted

604 at the apex of the tip (e.g. the virus is too high on the tip, preventing interactions to occur).
605 Experiments should then be performed with another tip. If this happens with most of the probes,
606 the concentration of the virus solution used to functionalize the tip should be increased, to increase
607 the probability of grafting a virion at the tip apex. If adhesion events are observed all over the cell
608 surface, the tip is probably contaminated with cellular debris from the viral solution. To overcome
609 this, insist on the centrifugation step prior to the virus coupling to the PEG spacer, or use a virus
610 solution with a higher purity.

611 6. Depending on the viral specie, one or multiple glycoprotein from the virus coat can be expected to
612 interact with specific receptors on the cell surface, resulting in different patterns of the Gaussian
613 rupture force distributions. When the virus-cell system probed contains only one type of
614 glycoprotein-receptor pair, the establishment of multiple bonds should appear as peaks in the force
615 distribution located at values that are multiple from the first (lowest force) peak, with the latter
616 that should correspond to single interactions. When multiple viral glycoproteins are involved in
617 cell binding, the attribution of different peaks to a specific glycoprotein is a challenging task, since
618 multiple interactions can occur with one, or a combination of different glycoproteins.

619

620

Acknowledgements

The research of the authors is financially supported by the Fonds National de la Recherche Scientifique (F.R.S.-FNRS grant number: PDR T.0070.16 to D.A.), the Université catholique de Louvain (Fonds Spéciaux de Recherche) and the 'Erwin Schroedinger Fellowship Abroad' (Austrian Science Fund (FWF), grant number J-4052 to M.K.). M.D. and D.A. are Research Fellow and Research Associate at the FRS-FNRS respectively.

629 **References**

630 1. Pelkmans L, Helenius A (2003) Insider information: what viruses tell us about endocytosis. Curr
631 Opin Cell Biol 15 (4):414-422

632 2. Boulant S, Stanifer M, Lozach PY (2015) Dynamics of virus-receptor interactions in virus binding,
633 signaling, and endocytosis. Viruses 7 (6):2794-2815

634 3. Carette JE, Guimaraes CP, Varadarajan M, Park AS, Wuethrich I, Godarova A, Kotecki M, Cochran
635 BH, Spooner E, Ploegh HL (2009) Haploid genetic screens in human cells identify host factors used by
636 pathogens. Science 326 (5957):1231-1235

637 4. Dimitrov DS (2004) Virus entry: molecular mechanisms and biomedical applications. Nat Rev
638 Microbiol 2 (2):109-122

639 5. Brandenburg B, Zhuang X (2007) Virus trafficking–learning from single-virus tracking. Nat Rev
640 Microbiol 5 5 (3):197

641 6. Smith AE, Helenius A (2004) How viruses enter animal cells. Science 304 (5668):237-242

642 7. Schnell MJ, Mebatsion T, Conzelmann KK (1994) Infectious rabies viruses from cloned cDNA. Embo
643 J 13 (18):4195-4203

644 8. Ghanem A, Kern A, Conzelmann KK (2012) Significantly improved rescue of rabies virus from cDNA
645 plasmids. Eur J Cell Biol 91 (1):10-16

646 9. Herrmann A, Sieben C (2015) Single-virus force spectroscopy unravels molecular details of virus
647 infection. Integr Biol (Camb) 7 (6):620-632

648 10. Matrosovich MN, Gambaryan AS (2012) Solid-phase assays of receptor-binding specificity.
649 Methods Mol Biol 865:71-94

650 11. Watanabe T, Kiso M, Fukuyama S, Nakajima N, Imai M, Yamada S, Murakami S, Yamayoshi S,
651 Iwatsuki-Horimoto K, Sakoda Y et al. (2013) Characterization of H7N9 influenza A viruses isolated
652 from humans. Nature 501 (7468):551-555

653 12. Shi Y, Zhang W, Wang F, Qi J, Wu Y, Song H, Gao F, Bi Y, Zhang Y, Fan Z et al. (2013) Structures and
654 receptor binding of hemagglutinins from human-infecting H7N9 influenza viruses. Science 342
655 (6155):243-247

656 13. Suenaga E, Mizuno H, Penmetcha KK (2012) Monitoring influenza hemagglutinin and glycan
657 interactions using surface plasmon resonance. Biosens Bioelectron 32 (1):195-201

658 14. Papp I, Sieben C, Ludwig K, Roskamp M, Bottcher C, Schlecht S, Herrmann A, Haag R (2010)
659 Inhibition of influenza virus infection by multivalent sialic-acid-functionalized gold nanoparticles.
660 Small 6 (24):2900-2906

661 15. Xiong X, Coombs PJ, Martin SR, Liu J, Xiao H, McCauley JW, Locher K, Walker PA, Collins PJ,
662 Kawaoka Y et al. (2013) Receptor binding by a ferret-transmissible H5 avian influenza virus. Nature
663 497 (7449):392-396

664 16. Roingeard P (2008) Viral detection by electron microscopy: past, present and future. Biol Cell 100
665 (8):491-501

666 17. Mercer J, Helenius A (2009) Virus entry by macropinocytosis. Nat Cell Biol 11 (5):510-520

667 18. Ando T, Uchihashi T, Kodera N (2013) High-speed AFM and applications to biomolecular systems.
668 Annu Rev Biophys 42:393-414

669 19. Kienberger F, Mueller H, Pastushenko V, Hinterdorfer P (2004) Following single antibody binding
670 to purple membranes in real time. EMBO Rep 5 (6):579-583

671 20. Hinterdorfer P, Dufrêne YF (2006) Detection and localization of single molecular recognition
672 events using atomic force microscopy. Nat Methods 3 (5):347-355

673 21. Neuman KC, Nagy A (2008) Single-molecule force spectroscopy: optical tweezers, magnetic
674 tweezers and atomic force microscopy. Nat Methods 5 (6):491-505

675 22. Sieben C, Kappel C, Zhu R, Wozniak A, Rankl C, Hinterdorfer P, Grubmüller H, Herrmann A (2012)
676 Influenza virus binds its host cell using multiple dynamic interactions. Proc Natl Acad Sci U S A 109
677 (34):13626-13631

678 23. Rankl C, Kienberger F, Wildling L, Wruss J, Gruber HJ, Blaas D, Hinterdorfer P (2008) Multiple
679 receptors involved in human rhinovirus attachment to live cells. Proc Natl Acad Sci U S A 105
680 (46):17778-17783

681 24. Chang MI, Panorchan P, Dobrowsky TM, Tseng Y, Wirtz D (2005) Single-molecule analysis of
682 human immunodeficiency virus type 1 gp120-receptor interactions in living cells. J Virol 79
683 (23):14748-14755

684 25. Dobrowsky TM, Zhou Y, Sun SX, Siliciano RF, Wirtz D (2008) Monitoring early fusion dynamics of
685 human immunodeficiency virus type 1 at single-molecule resolution. J Virol 82 (14):7022-7033

686 26. Binnig G, Quate CF, Gerber C (1986) Atomic force microscope. Phys Rev Lett 56 (9):930-933

687 27. Muller DJ, Helenius J, Alsteens D, Dufrene YF (2009) Force probing surfaces of living cells to
688 molecular resolution. Nat Chem Biol 5 (6):383-390

689 28. Dufrene YF, Martinez-Martin D, Medalsy I, Alsteens D, Muller DJ (2013) Multiparametric imaging
690 of biological systems by force-distance curve-based AFM. Nat Methods 10 (9):847-854

691 29. Hörber J, Miles M (2003) Scanning probe evolution in biology. Science 302 (5647):1002-1005

692 30. Engel A, Müller DJ (2000) Observing single biomolecules at work with the atomic force
693 microscope. Nat Struct Mol Biol 7 (9):715-718

694 31. Dufrene YF, Ando T, Garcia R, Alsteens D, Martinez-Martin D, Engel A, Gerber C, Muller DJ (2017)
695 Imaging modes of atomic force microscopy for application in molecular and cell biology. Nat
696 Nanotechnol 12 (4):295-307

697 32. Kienberger F, Kada G, Mueller H, Hinterdorfer P (2005) Single molecule studies of antibody–
698 antigen interaction strength versus intra-molecular antigen stability. J Mol Biol 347 (3):597-606

699 33. Radmacher M (2002) Measuring the elastic properties of living cells by the atomic force
700 microscope. Methods Cell Biol 68 (1):67-90

701 34. Viani MB, Pietrasanta LI, Thompson JB, Chand A, Gebeshuber IC, Kindt JH, Richter M, Hansma HG,
702 Hansma PK (2000) Probing protein-protein interactions in real time. Nat Struct Biol 7 (8):644-647

703 35. Kuznetsov YG, Malkin A, Lucas R, Plomp M, McPherson A (2001) Imaging of viruses by atomic
704 force microscopy. J Gen Virol 82 (9):2025-2034

705 36. Alsteens D, Newton R, Schubert R, Martinez-Martin D, Delguste M, Roska B, Muller DJ (2017)
706 Nanomechanical mapping of first binding steps of a virus to animal cells. Nat Nanotechnol 12 (2):177-
707 183

708 37. Gerber C, Lang HP (2006) How the doors to the nanoworld were opened. Nat Nanotechnol 1
709 (1):3-5

710 38. Sieben C, Herrmann A (2017) Single virus force spectroscopy: The ties that bind. Nat Nanotechnol
711 12 (2):102-103

712 39. Henderson E, Haydon PG, Sakaguchi DS (1992) Actin filament dynamics in living glial cells imaged
713 by atomic force microscopy. Science 257 (5078):1944-1946

714 40. Hoh JH, Schoenenberger CA (1994) Surface morphology and mechanical properties of MDCK
715 monolayers by atomic force microscopy. J Cell Sci 107 (Pt 5) (5):1105-1114

716 41. Hoh JH, Lal R, John SA, Revel JP, Arnsdorf MF (1991) Atomic force microscopy and dissection of
717 gap junctions. Science 253 (5026):1405-1408

718 42. Mou J, Yang J, Shao Z (1995) Atomic force microscopy of cholera toxin B-oligomers bound to
719 bilayers of biologically relevant lipids. J Mol Biol 248 (3):507-512

720 43. Schabert FA, Henn C, Engel A (1995) Native Escherichia coli OmpF porin surfaces probed by
721 atomic force microscopy. Science 268 (5207):92-94

722 44. Hansma HG, Vesenka J, Siegerist C, Kelderman G, Morrett H, Sinsheimer RL, Elings V, Bustamante
723 C, Hansma PK (1992) Reproducible imaging and dissection of plasmid DNA under liquid with the
724 atomic force microscope. Science 256 (5060):1180-1184

725 45. Hoh JH, Sosinsky GE, Revel JP, Hansma PK (1993) Structure of the extracellular surface of the gap
726 junction by atomic force microscopy. Biophys J 65 (1):149-163

727 46. Müller D, Schabert FA, Büldt G, Engel A (1995) Imaging purple membranes in aqueous solutions
728 at sub-nanometer resolution by atomic force microscopy. Biophys J 68 (5):1681-1686

729 47. Karrasch S, Dolder M, Schabert F, Ramsden J, Engel A (1993) Covalent binding of biological
730 samples to solid supports for scanning probe microscopy in buffer solution. Biophys J 65 (6):2437-
731 2446

732 48. Putman CA, Van der Werf KO, De Grooth BG, Van Hulst NF, Greve J (1994) Tapping mode atomic
733 force microscopy in liquid. Appl Phys Lett 64 (18):2454-2456

734 49. Wegmann S, Jung YJ, Chinnathambi S, Mandelkow E-M, Mandelkow E, Muller DJ (2010) Human
735 Tau isoforms assemble into ribbon-like fibrils that display polymorphic structure and stability. J Biol
736 Chem 285 (35):27302-27313

737 50. Ido S, Kimura K, Oyabu N, Kobayashi K, Tsukada M, Matsushige K, Yamada H (2013) Beyond the
738 helix pitch: direct visualization of native DNA in aqueous solution. ACS Nano 7 (2):1817-1822

739 51. Ido S, Kimiya H, Kobayashi K, Kominami H, Matsushige K, Yamada H (2014) Immunoactive two-
740 dimensional self-assembly of monoclonal antibodies in aqueous solution revealed by atomic force
741 microscopy. Nat Mater 13 (3):264-270

742 52. Hansma HG, Hoh JH (1994) Biomolecular imaging with the atomic force microscope. Annu Rev
743 Biophys Biomol Struct 23 (1):115-139

744 53. Ohnesorge F, Hörber J, Häberle W, Czerny C, Smith D, Binnig G (1997) AFM review study on pox
745 viruses and living cells. Biophys J 73 (4):2183-2194

746 54. YuG K, Malkin A, Land T, DeYoreo J, Barba A, Konnert J, McPherson A (1997) Molecular resolution
747 imaging of macromolecular crystals by atomic force microscopy. Biophys J 72 (5):2357-2364

748 55. Drygin YF, Bordunova OA, Gallyamov MO, Yaminsky IV (1998) Atomic force microscopy
749 examination of tobacco mosaic virus and virion RNA. FEBS letters 425 (2):217-221

750 56. Kienberger F, Zhu R, Moser R, Rankl C, Blaas D, Hinterdorfer P (2004) Dynamic force microscopy
751 for imaging of viruses under physiological conditions. Biol Proced Online 6 (1):120

752 57. Malkin AJ, Plomp M, McPherson A (2005) Unraveling the architecture of viruses by high-
753 resolution atomic force microscopy. DNA Viruses: Methods and Protocols:85-108

754 58. Kasas S, Longo G, Dietler G (2013) Mechanical properties of biological specimens explored by
755 atomic force microscopy. Journal of Physics D: Applied Physics 46 (13):133001

59. Mateu MG (2012) Mechanical properties of viruses analyzed by atomic force microscopy: a virological perspective. Virus research 168 (1):1-22

60. Martinez-Martin D, Carrasco C, Hernando-Perez M, De Pablo PJ, Gomez-Herrero J, Perez R, Mateu MG, Carrascosa JL, Kiracofe D, Melcher J (2012) Resolving structure and mechanical properties at the nanoscale of viruses with frequency modulation atomic force microscopy. PLoS One 7 (1):e30204

61. Kuznetsov YG, Victoria J, Robinson W, McPherson A (2003) Atomic force microscopy investigation of human immunodeficiency virus (HIV) and HIV-infected lymphocytes. J Virol 77 (22):11896-11909

62. Parachoniak CA, Park M (2012) Dynamics of receptor trafficking in tumorigenicity. Trends Cell Biol 22 (5):231-240

63. Matias V, Beveridge T (2005) Cryoelectron microscopy reveals native polymeric cell wall structure in. Bacillus subtilis 168:240-251

64. Hell SW (2007) Far-field optical nanoscopy. Science 316 (5828):1153-1158

65. Fornasiero EF, Rizzoli SO (2014) Super-resolution microscopy techniques in the neurosciences. Springer,

66. Boonaert CJ, Rouxhet PG (2000) Surface of lactic acid bacteria: relationships between chemical composition and physicochemical properties. Appl Environ Microbiol 66 (6):2548-2554

67. Dufrêne YF, Boonaert CJ, Gerin PA, Asther M, Rouxhet PG (1999) Direct Probing of the Surface Ultrastructure and Molecular Interactions of Dormant and Germinating Spores ofPhanerochaete chrysosporium. J Bacteriol 181 (17):5350-5354

68. Kasas S, Ikai A (1995) A method for anchoring round shaped cells for atomic force microscope imaging. Biophys J 68 (5):1678-1680

69. Dague E, Alsteens D, Latge JP, Verbelen C, Raze D, Baulard AR, Dufrene YF (2007) Chemical force microscopy of single live cells. Nano Lett 7 (10):3026-3030

70. Dague E, Alsteens D, Latge JP, Dufrene YF (2008) High-resolution cell surface dynamics of germinating Aspergillus fumigatus conidia. Biophys J 94 (2):656-660

71. Touhami A, Jericho MH, Beveridge TJ (2004) Atomic force microscopy of cell growth and division in Staphylococcus aureus. J Bacteriol 186 (11):3286-3295

72. Butt H-J, Cappella B, Kappl M (2005) Force measurements with the atomic force microscope: Technique, interpretation and applications. Surf Sci Rep 59 (1):1-152

73. Hinterdorfer P, Baumgartner W, Gruber HJ, Schilcher K, Schindler H (1996) Detection and localization of individual antibody-antigen recognition events by atomic force microscopy. Proc Natl Acad Sci U S A 93 (8):3477-3481

74. Ludwig M, Dettmann W, Gaub HE (1997) Atomic force microscope imaging contrast based on molecular recognition. Biophys J 72 (1):445-448

75. Wildling L, Unterauer B, Zhu R, Rupprecht A, Haselgrubler T, Rankl C, Ebner A, Vater D, Pollheimer P, Pohl EE et al. (2011) Linking of sensor molecules with amino groups to amino-functionalized AFM tips. Bioconjug Chem 22 (6):1239-1248

76. Puntheeranurak T, Neundlinger I, Kinne RKH, Hinterdorfer P (2011) Single-molecule recognition force spectroscopy of transmembrane transporters on living cells. Nat Protocols 6 (9):1443-1452

77. Evans EA, Calderwood DA (2007) Forces and bond dynamics in cell adhesion. Science 316 (5828):1148-1153

78. Evans E, Ritchie K (1997) Dynamic strength of molecular adhesion bonds. Biophys J 72 (4):1541-1555

799 79. Alsteens D, Dupres V, Yunus S, Latgé J-P, Heinisch JrJ, Dufrêne YF (2012) High-resolution imaging
800 of chemical and biological sites on living cells using peak force tapping atomic force microscopy.
801 Langmuir 28 (49):16738-16744

802 80. Pfreundschuh M, Martinez-Martin D, Mulvihill E, Wegmann S, Muller DJ (2014) Multiparametric
803 high-resolution imaging of native proteins by force-distance curve-based AFM. Nat Protoc 9 (5):1113-
804 1130

805 81. Bell GI (1978) Models for the specific adhesion of cells to cells. Science 200 (4342):618-627

806 82. Collin D, Ritort F, Jarzynski C, Smith SB, Tinoco I, Jr., Bustamante C (2005) Verification of the
807 Crooks fluctuation theorem and recovery of RNA folding free energies. Nature 437 (7056):231-234

808 83. Friddle RW, Noy A, De Yoreo JJ (2012) Interpreting the widespread nonlinear force spectra of
809 intermolecular bonds. Proc Natl Acad Sci U S A 109 (34):13573-13578

810 84. Carneiro FA, Lapido-Loureiro PA, Cordo SM, Stauffer F, Weissmüller G, Bianconi ML, Juliano MA,
811 Juliano L, Bisch PM, Poian ATD (2006) Probing the interaction between vesicular stomatitis virus and
812 phosphatidylserine. Eur Biophys J 35 (2):145-154

813 85. Liu N, Peng B, Lin Y, Su Z, Niu Z, Wang Q, Zhang W, Li H, Shen J (2010) Pulling genetic RNA out of
814 tobacco mosaic virus using single-molecule force spectroscopy. J Am Chem Soc 132 (32):11036-
815 11038

816 86. Korneev D, Popova A, Generalov V, Zaitsev B (2016) Atomic force microscopy-based single virus
817 particle spectroscopy. Biophysics 61 (3):413-419

818 87. Wörmann X, Lesch M, Welke R-W, Okonechnikov K, Abdurishid M, Sieben C, Geissner A,
819 Brinkmann V, Kastner M, Karner A (2016) Genetic characterization of an adapted pandemic 2009
820 H1N1 influenza virus that reveals improved replication rates in human lung epithelial cells. Virology
821 492:118-129

822 88. Schillers H, Medalsy I, Hu S, Slade AL, Shaw JE (2016) PeakForce Tapping resolves individual
823 microvilli on living cells. J Mol Recognit 29 (2):95-101

824 89. Huhti L, Blazevic V, Nurminen K, Koho T, Hytonen VP, Vesikari T (2010) A comparison of methods
825 for purification and concentration of norovirus GII-4 capsid virus-like particles. Arch Virol 155
826 (11):1855-1858

827 90. Hutornojs V, Niedre-Otomere B, Kozlovska T, Zajakina A (2012) Comparison of ultracentrifugation
828 methods for concentration of recombinant alphaviruses: sucrose and iodixanol cushions. Environ Exp
829 Biol 10:117-123

830 91. Viani MB, Schäffer TE, Chand A, Rief M, Gaub HE, Hansma PK (1999) Small cantilevers for force
831 spectroscopy of single molecules. J Appl Phys 86 (4):2258-2262

832 92. Gruber H (2016) Crosslinkers and Protocols for AFM Tip Functionalization.
833 http://www.jku.at/biophysics/content/e257042. Accessed 22.08.2016 2016

834 93. Ebner A, Hinterdorfer P, Gruber HJ (2007) Comparison of different aminofunctionalization
835 strategies for attachment of single antibodies to AFM cantilevers. Ultramicroscopy 107 (10-11):922-
836 927

837 94. Kienberger F, Pastushenko VP, Kada G, Gruber HJ, Riener C, Schindler H, Hinterdorfer P (2000)
838 Static and Dynamical Properties of Single Poly(Ethylene Glycol) Molecules Investigated by Force
839 Spectroscopy. Single Molecules 1 (2):123-128

840 95. Butt HJ, Jaschke M (1995) Calculation of thermal noise in atomic force microscopy.
841 Nanotechnology 6 (1):1-7

96. Florin E-L, Rief M, Lehmann H, Ludwig M, Dornmair C, Moy VT, Gaub HE (1995) Sensing specific molecular interactions with the atomic force microscope. Biosensors Bioelectron 10 (9):895-901

97. Hutter JL, Bechhoefer J (1993) Calibration of atomic-force microscope tips. Rev Sci Instrum 64 (7):1868-1873

98. te Riet J, Katan AJ, Rankl C, Stahl SW, van Buul AM, Phang IY, Gomez-Casado A, Schon P, Gerritsen JW, Cambi A et al. (2011) Interlaboratory round robin on cantilever calibration for AFM force spectroscopy. Ultramicroscopy 111 (12):1659-1669

99. Sader JE, Borgani R, Gibson CT, Haviland DB, Higgins MJ, Kilpatrick JI, Lu J, Mulvaney P, Shearer CJ, Slattery AD et al. (2016) A virtual instrument to standardise the calibration of atomic force microscope cantilevers. Rev Sci Instrum 87 (9):093711

100. Gates RS, Osborn WA, Shaw GA (2015) Accurate flexural spring constant calibration of colloid probe cantilevers using scanning laser Doppler vibrometry. Nanotechnology 26 (23):235704

101. Bustamante C, Marko JF, Siggia ED, Smith S (1994) Entropic elasticity of lambda-phage DNA. Science 265 (5178):1599-1600

102. Friedsam C, Wehle AK, Kühner F, Gaub HE (2003) Dynamic single-molecule force spectroscopy: bond rupture analysis with variable spacer length. J Phys: Condens Matter 15 (18):S1709

103. Bizzarri AR, Cannistraro S (2010) The application of atomic force spectroscopy to the study of biological complexes undergoing a biorecognition process. Chem Soc Rev 39 (2):734-749

104. Hane FT, Attwood SJ, Leonenko Z (2014) Comparison of three competing dynamic force spectroscopy models to study binding forces of amyloid-beta (1-42). Soft Matter 10 (12):1924-1930

105. Alsteens D, Pfreundschuh M, Zhang C, Spoerri PM, Coughlin SR, Kobilka BK, Müller DJ (2015) Imaging G protein-coupled receptors while quantifying their ligand-binding free-energy landscape. Nat Methods 12 (9):845-851

106. Sulchek T, Friddle RW, Noy A (2006) Strength of multiple parallel biological bonds. Biophys J 90 (12):4686-4691

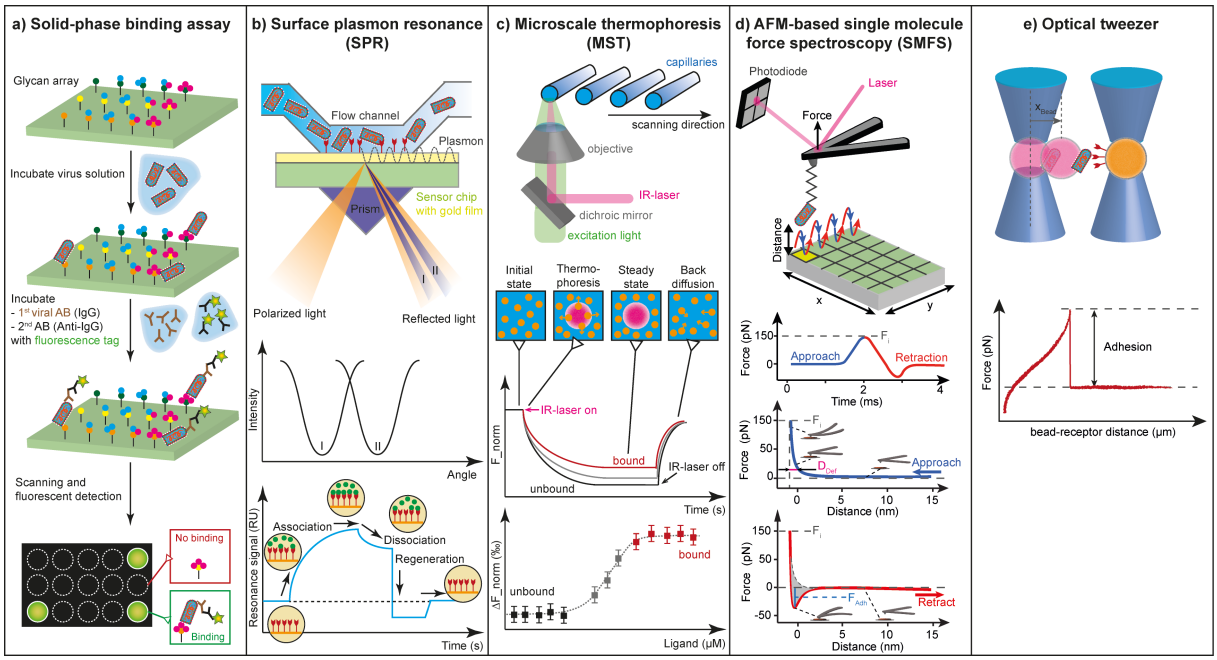

Figure 1. Overview of current methods available to study virus-receptors interaction. (a)-(c) Ensemble binding assays: (a) Solid-phase binding assay, where the investigated receptor is coupled to a flat surface and allowed to interact with intact viruses. By utilizing a "sandwich"-building approach, virus binding is detected via fluorescently labeled secondary antibodies. **(b)** Surface plasmon resonance (SPR) is used to obtain thermodynamic properties of virus-receptor binding. The receptor molecules are flushed into a chamber, where they interact with a gold-coated sensor-chip. Subsequent flushing of the virus into this chamber allows determining association and dissociation kinetics by following the time *vs.* resonance signal curve. **(c)** Microscale thermophoresis makes it possible to measure binding and unbinding kinetics in solution under defined, controlled conditions. Microscale thermophoresis is the directed movement of particles in a microscopic temperature gradient. Any change in the hydration shell of biomolecules due to changes in their structure/ conformation (*e.g.* after virus binding) results in a negative change of the movement along the temperature gradient and thus can be used to determine binding affinities. **(d,e) Single-molecule techniques: (d)** AFM-based single molecule force spectroscopy can be utilized to determine inter-molecular forces by repeatedly approaching and withdrawing a virus-functionalized AFM tip to their respective (cell surface) receptors in z-direction. **(e)** Optical tweezers are instruments that use a highly focused laser beam to provide an attractive or repulsive force, depending on the refractive index mismatch to physically hold and/or move microscopic dielectric objects similar to tweezers.

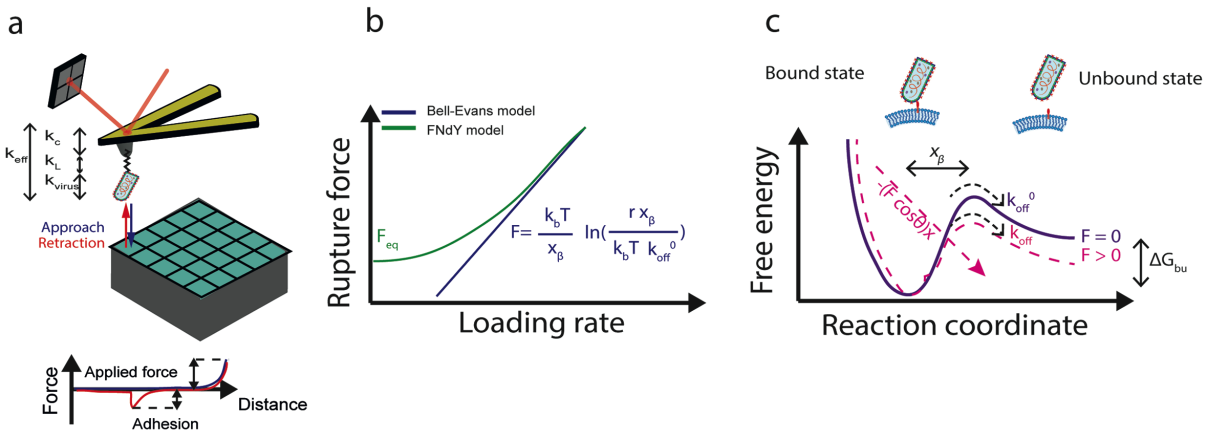

Figure 2. Force-distance curve-based AFM and extraction of kinetic and thermodynamic properties of receptor-ligand bonds. (a) During each approach-retraction cycle, the AFM tip grafted with a single viral particle records a force versus distance curve, on which adhesion events between the probe and the sample can be observed. **(b)** Reporting the measured rupture force as a function of the loading rate that allows quantitative kinetic and thermodynamic parameters of the virus-receptor interaction to be extracted. To do so, the effective spring constant of the force transducer system can be evaluated by considering its different components as springs in series (a) (see text for details). **(c)** Free energy potential separating bound and unbound states of a virus-cell receptor system in the absence (purple) and in the presence of an externally applied pulling force (dashed, pink). The external force tilts the energy landscape towards the dissociation of the interacting complex, reducing the energy barrier.

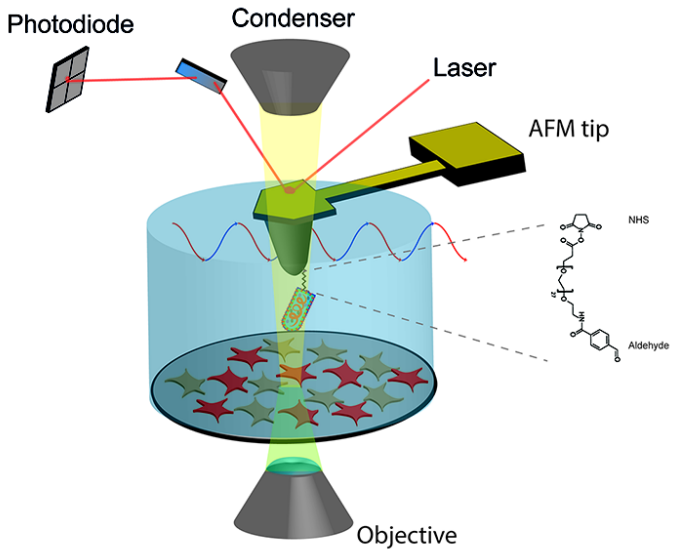

902

903 **Figure 3. Combined atomic force and fluorescence microscopy set-up for the investigation of virus-cell**
904 **receptor interactions.** A Petri dish containing mixed fluorescent cells expressing a particular receptor and non-
905 fluorescent cells that do not express the receptor is placed on an inverted optical fluorescence microscope. A
906 virus particle is grafted to the AFM tip by means of an heterobifunctional PEG linker, which can then be
907 oscillated over the confluent monolayer, to record virus-cell interactions.

908

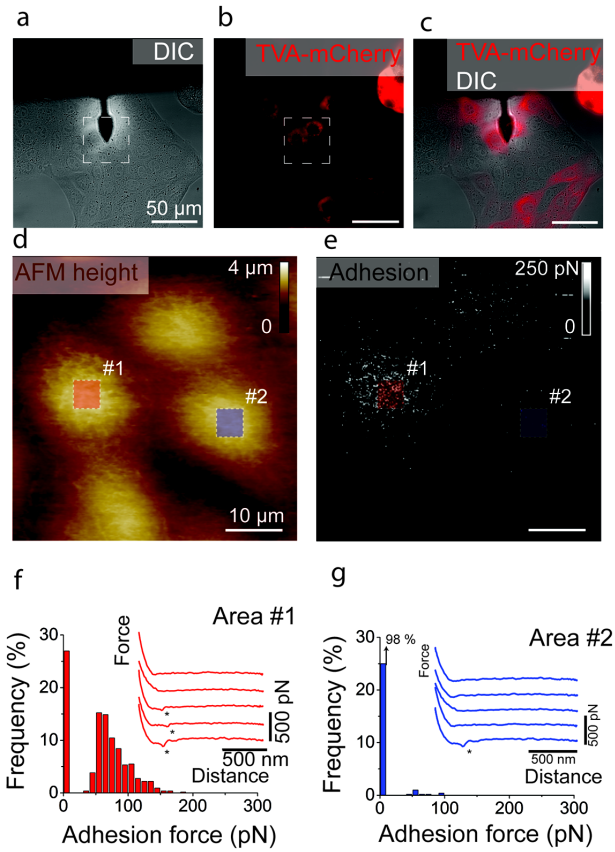

Figure 4. FD-based AFM investigation of virus binding site to living MDCK cells (a-c), DIC image, fluorescence channel and superimposition of both images showing the confluent layer of cells expressing TVA-mCherry receptor surrounded with control cells. The AFM tip is placed above the region of interest. **(d,e)** FD-based AFM height image and adhesion map of cells recorded in the dashed square shown in **(a,b). (f,g)**, Distribution of adhesion forces measured between the virus-derivatized AFM tip and two areas of cells highlighted in **(d,e)**. The adhesion force of the last peak (asterisk) can be extracted for further analysis. The red data (area #1) are extracted from cells expressing the TVA receptor (as shown on the fluorescence channel) and the blue data (area #2) are from control cells. Insets show, representative force-distance curves with asterisks indicating maximum adhesion peaks.

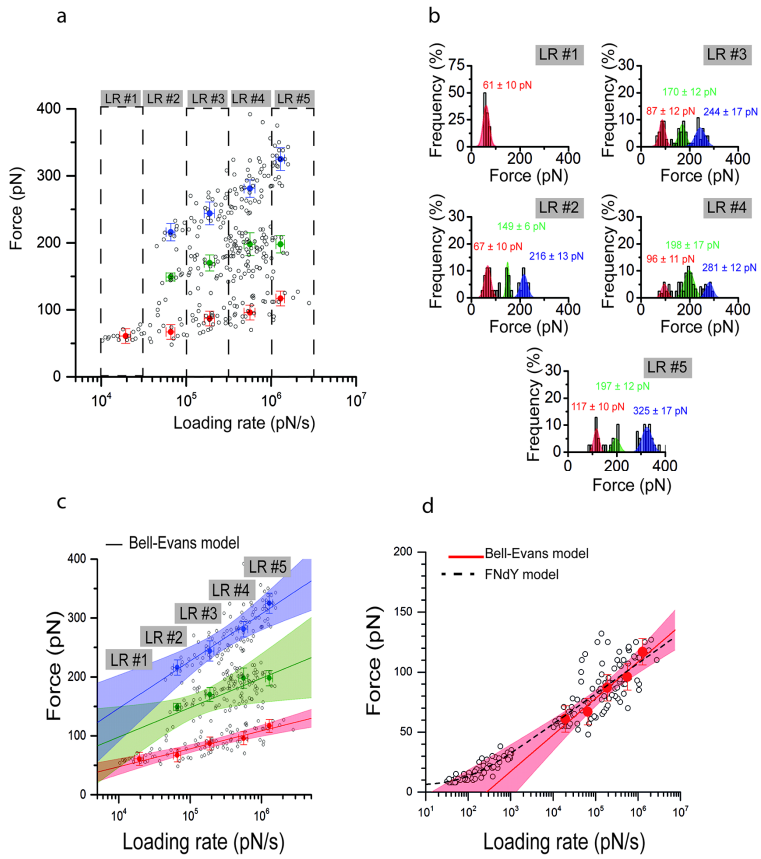

Figure 5. Extraction of kinetic and thermodynamic parameters of virus-receptor interactions. (a) Dynamic force spectroscopy (DFS) plot showing the force required to separate the virus from the cell surface. The forces of single virus-receptor rupture events (circles) are plotted against the *LR*. **(b)**, Small *LR* ranges #1–#5 are binned and the distributions of the rupture forces are plotted as histograms. This classification reveals multiple force peaks with average values corresponding to single (red), double (green) or triple (blue) simultaneously established virus-receptor interactions. The average values of the force distributions are extracted and plotted on the DFS plot **(a)**, enabling their analysis using the Bell-Evans model **(c)**. **(d)** Probing the rupture force of the system at reduced loading rate allows to gain insights into thermodynamic properties of the virus-receptor bonds, by fitting the data with the Friddle-Noy-de-Yoreo model (see text for details).